Hindawi
Wireless Communications and Mobile Computing
Volume 2022, Article ID 5932553, 11 pages
https://doi.org/10.1155/2022/5932553

Research Article

Optimal Design of Interleaved Subconnected Hybrid Structure for mmWave Massive MIMO Systems

Xiaoxiao Gu,[1,2] **Jinyan Qi**,[1,2] **Wence Zhang**,[1,2] **Xianglan Dong**,[3] **Xu Bao**,[1,2] **and Jing Xia**[1,2]

[1]*School of Computer Science and Communication Engineering, Jiangsu University, Zhenjiang, China*
[2]*Jiangsu Key Laboratory of Security Technology for Industrial Cyberspace, Zhenjiang, China*
[3]*Shijiazhuang Tiedao University, Shijiazhuang, China*

Correspondence should be addressed to Wence Zhang; wencezhang@ujs.edu.cn

Received 12 April 2022; Revised 9 August 2022; Accepted 26 August 2022; Published 13 September 2022

Academic Editor: Daniele Pinchera

Massive multiple-input multiple-output (MIMO) systems based on millimeter-wave (mmWave) technology commonly utilize a combination of hybrid analog and digital signal processing to reduce the number of radiofrequency (RF) chains, cutting down the hardware costs and power consumption. The subconnected structure is one of the architectures that realize hybrid analog and digital processing, in which each RF chain is connected to a subset of antennas through phase shifters so as to reduce the implementation complexity. In this paper, we investigate the best subconnected structure design for mmWave massive MIMO systems. First, we formulate the optimization problem based on a simplified connection model. Next, we derive a suboptimal solution in closed form by leveraging the mmWave channel characteristics and discuss the impact of different connection parameters on the spectral efficiency. The spectral efficiency is closely related to the structure of the analog processing and the interantenna spacing. When the interantenna spacing is an even a multiple of half wavelength, the localized structure, i.e., $i = 1$ achieves the maximum spectral efficiency. When the interantenna spacing is an odd multiple of half wavelength and the analog processing is accomplished by $i = 2$ interleaved structure, the best performance is obtained. Numerical results demonstrate the correctness of the theoretical analysis.

1. Introduction

In the future generation of mobile communication systems, millimeter-wave (mmWave) combined with massive multiple-input multiple-output (MIMO) has been intensively envisaged as a promising technology [1–5], because of sufficient available spectrum resources which help to obtain higher data rates. Meanwhile, the high beamforming gains attributed to massive MIMO could overcome the extreme path loss of mmWave communications [6, 7]. However, the traditional full-digital structure that connects each antenna with a radio-frequency (RF) chain is not desirable for mmWave massive MIMO systems because of the high hardware cost and power consumption [8, 9].

By linking the antennas to far fewer RF chains via a phase shifter network, hybrid analog and digital signal processing provides a viable approach for mmWave massive MIMO communication, which is accomplished in the analog domain followed by baseband processing in the digital domain [10]. The system performance of the hybrid structure can be close to that of the full-digital structure [11–13].

According to the connection topology between antennas and RF chains, the hybrid structure is divided into two types in general. For the fully connected structure, each RF chain is linked to all antennas. In contrast, for subconnected structures, an RF chain is only connected to a subarray of the total available antennas [14]. The performance of the subconnected structure is slightly lower than that of the fully connected structure, but it can be more energy-efficient by reducing the number of phase shifters [14, 15]. The subconnected structure achieves a trade-off between the system performance and hardware complexity. Based on the configuration of the

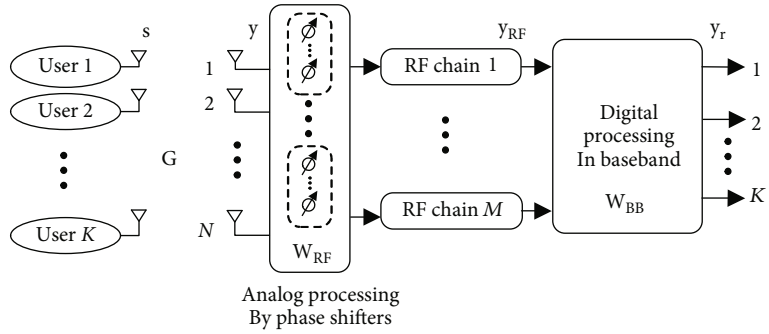

Figure 1: mmWave Massive MIMO system with hybrid analog and digital processing.

antenna subarray, the subconnected structure is classified into two categories, localized structure and interleaved structure. For the localized structures, the elements in an antenna subarray are adjacent and consecutive [14–17], while they are separated in the interleaved structure.

The interleaved structure is one of the most popular structures [8, 18–28]. It is proved that the angle of arrival (AoA) estimation of interleaved structure could converge faster with lower complexity [29–31]. The interleaved structure can eliminate the grating lobes as well as achieve multiple beams with high gain by adopting interleaved coding schemes [18–20], [24], hence to reduce interference and achieve high signal to interference ratio (SIR). Moreover, the interleaved structure could also achieve high-speed communication even in densely populated areas [20].

The interleaved structure is first proposed in [29]. In [18, 19, 21–25] and [29–32], the authors studied the fixed structures interleaved with a constant number of elements. In [20, 26], arbitrary interleaved structures are proposed. In [27, 28], the antenna subarrays of the interleaved structures have the same size and are not allowed to overlap, which is different from the overlapped structure. In [18, 25], some prototype of interleaved structure in mmWave frequencies is realized through a phased array chip. In [31, 33], the spectral efficiency of the localized structure and the interleaved structure are compared. In [33], the performance of the interleaved structure with constant configuration of subarray is developed. The authors of [31] consider the influence of subarray configuration on the spectral efficiency. It shows that different configurations significantly affect the overall performance. However, existing works do not provide results on the optimal interleaved structure and the impact of connection parameters on the system performance.

In this paper, we consider the uplink of the mmWave massive MIMO system as shown in Figure 1, where the hybrid analog and digital signal processing is adopted. We compare the spectral efficiency of diverse subconnected structures, study the main parameters that affect the system performance, and derive the optimal structure in closed form. The main contributions of this paper are as follows:

(i) We derive the suboptimal interleaved structure in closed form for channels with a single propagation path, and then the results are extended to the case with multiple propagation paths based on the properties of mmWave channel

(ii) We propose an efficient algorithm to find the optimal interleaved structure that maximizes the spectral efficiency

(iii) We study the impact of interleave factor (i) and interantenna spacing (d) on the spectral efficiency. The interleaved structure with $i = 2$ achieves the best performance when the interantenna spacing is an odd multiple of half wavelength. The localized structure achieves the best performance when the interantenna spacing is an even a multiple of half wavelength

The remainder of the paper is organized as follows. In Section 2, we give the system model and formulate the optimization problem for finding the optimal subconnected structure. In Section 3, we obtain the optimal interleaved structure by leveraging the characteristics of the mmWave channel. In Section 4, numerical results are provided. Finally, Section 5 draws conclusions.

Notations: vectors and matrices are denoted by boldface lower and uppercase letters, respectively. $\mathscr{D}$ represents a set. $(\cdot)^{\mathrm{H}}$ denotes the conjugate transpose, and $(\cdot)^{-1}$ denotes the inverse of a matrix. Expectation and determinant operators are denoted by $\mathbb{E}(\cdot)$ and $\det(\cdot)$, respectively. The diagonal matrix is denoted by $\mathrm{diag}(\varepsilon_1, \varepsilon_2, \cdots, \varepsilon_K)$ with diagonal entries represented by ε_k, $k = 1, 2, \cdots, K$. $\mathbf{I}_K$ denotes an $K \times K$ identity matrix. $\mathscr{CN}(\mathbf{0}, \mathbf{I}_N)$ denotes a complex Gaussian random vector, where the mean is $\mathbf{0}$ and the covariance matrix is $\mathbf{I}_N$.

2. System Model and Problem Formulation

In this section, we describe the signal model of the mmWave massive MIMO system and the connection between RF chains and antennas. Then, the optimization problem of the subconnected structure is formulated. Consider the uplink of a multiuser mmWave massive MIMO system which comprises of a base station (BS) with a uniform linear array (ULA) of N antennas and K single antennas utilizing resources at the same time and frequency. The considered hybrid processing subconnected structure at the BS is illustrated in Figure 1, which has two successive subprocedures:

analog processing and baseband processing. The N antennas and the M RF chains are connected arbitrarily through a phase shifter network which enables analog processing. The output of the RF chains is sent to the baseband for digital processing. To ensure the multiple data stream communication, we assume that the number of RF chains is equal to users, i.e., $M = K$. The received signal vector $\mathbf{y} \in \mathbb{C}^{N\times 1}$ at the BS can be presented as follows:

$$\mathbf{y} = \mathrm{GPs} + \mathbf{n}, \tag{1}$$

where $\mathbf{G} \in \mathbb{C}^{N\times K}$ denotes the channel matrix from users to the BS; $\mathbf{P} = \mathrm{diag}\,(\sqrt{p_1}, \sqrt{p_2}, \cdots, \sqrt{p_K})$, with p_k being the transmit power of the k-th user, $k = 1, 2, \cdots, K$; $\mathbf{s} \in \mathbb{C}^{K\times 1}$ is the transmit signal vector, and $\mathbf{n} \in \mathbb{C}^{N\times 1}$ is the additive white Gaussian noise (AWGN) vector, which follows the distribution of $\mathscr{CN}(\mathbf{0}, \mathbf{I}_N)$. Consider the large-scale fading, and the channel is modeled as

$$G = \mathrm{HD}^{1/2}, \tag{2}$$

where $D = \mathrm{diag}\,(\varepsilon_1, \varepsilon_2, \cdots, \varepsilon_K)$, and ε_k is the large-scale fading coefficient of the k-th user to the BS; $\mathbf{H} \in \mathbb{C}^{N\times K}$ is composed of the small-scale fading channel coefficients of all K users, and it can be presented as

$$\mathbf{H} = [\mathbf{h}_1, \mathbf{h}_2, \cdots, \mathbf{h}_K], \tag{3}$$

where $\mathbf{h}_k \in \mathbb{C}^{N\times 1}$ is the channel vector of the k-th user to the BS. Different from the low-frequency band, the number of scatters in the mmWave propagation environment is limited, and the correlation between different antennas is high. Therefore, the expanded Saleh-Valenzuela channel model in [9] for the mmWave propagation environment is adopted. Thus, $h_k \in \mathbb{C}^{N\times 1}$ can be modeled as

$$\mathbf{h}_k = \sqrt{\frac{N}{L}} \sum_{l=1}^{L} \alpha_{kl} \mathbf{a}(\phi_{kl}), \tag{4}$$

where L is the number of valid transmission paths from the k-th user to the BS; $\alpha_{kl} \sim \mathscr{CN}(0, 1)$ and $\phi_{kl} \in [0, 2\pi]$ are the complex gain and the AoA of the l-th propagation path of the k-th user, respectively. For the ULA, the steering vector $a(\phi_{kl}) \in \mathbb{C}^{N\times 1}$ is given by

$$\mathbf{a}(\phi_{kl}) = \frac{1}{\sqrt{N}} \left[1, \mathrm{e}^{-\mathrm{j}\Delta d \cos \phi_{kl}}, \cdots, \mathrm{e}^{-\mathrm{j}\Delta d(N-1) \cos \phi_{kl}}\right]^{\mathrm{T}}, \tag{5}$$

where d is the distance between adjacent antennas and $\Delta = 2\pi/\lambda$, and λ is the wavelength. Because of the near-far effect, the power of different users at the BS is different. To obtain the consistent received signal power $p = \varepsilon_k p_k$, a power control scheme is adopted in the uplink [34]. Hence, (1) can be rewritten as

$$\mathbf{y} = \sqrt{p}\mathbf{H}\mathbf{s} + \mathbf{n}. \tag{6}$$

To recover $\mathbf{s}$ at the BS with low power consumption and hardware cost, we focus on the hybrid processing scheme which has gained great research interest [10, 14–17]. As shown in Figure 1, the received signal vector after analog processing can be presented as

$$\mathbf{y}_{\mathrm{RF}} = \sqrt{p} W_{\mathrm{RF}}^{\mathrm{H}} H \mathbf{s} + \mathbf{W}_{\mathrm{RF}}^{\mathrm{H}} \mathbf{n} = \sqrt{p} H_{\mathrm{RF}} \mathbf{s} + \mathbf{W}_{\mathrm{RF}}^{\mathrm{H}} \mathbf{n}, \tag{7}$$

where $\mathbf{W}_{\mathrm{RF}} \in \mathbb{C}^{N\times M}$ is the analog processing matrix, which is realized by the phase shifter network and $H_{\mathrm{RF}} = W_{\mathrm{RF}}^{\mathrm{H}} H$ is the equivalent RF channel. Denote $\mathbf{W}_{\mathrm{BB}} \in \mathbb{C}^{M\times K}$ as the baseband processing matrix, and the received signal after baseband processing is given by

$$\mathbf{y}_{\mathrm{r}} = \sqrt{p} \mathbf{W}_{\mathrm{BB}}^{H} \mathbf{W}_{\mathrm{RF}}^{H} \mathbf{H}\mathbf{s} + \mathbf{W}_{\mathrm{BB}}^{H} \mathbf{W}_{\mathrm{RF}}^{H} \mathbf{n}. \tag{8}$$

The optimal connection between the RF links and the antenna array that maximizes the sum rate R of all users is very difficult to derive, due to its complicated expression. Besides, the connections only affect the analog processing. To simplify the problem at hand, we denote the mutual information of the link $s \longrightarrow y_{\mathrm{RF}}$ as $I(s, y_{\mathrm{RF}})$. Based on information theory, we have

$$R \le I(s, y_{\mathrm{RF}}) \le C, \tag{9}$$

where C is the channel capacity for channel matrix $\mathbf{G}$. $I(s, y_{\mathrm{RF}})$ is the upper bound of the sum rate R. Therefore, the optimization problem for R is altered to optimize $I(s, y_{\mathrm{RF}})$, which is given by

$$I(s, y_{\mathrm{RF}}) = \mathbb{E} \log_2 \det \left(\mathbf{I}_K + p\mathbf{R}_{\mathrm{n}_{\mathrm{RF}}}^{-1} \mathbf{W}_{\mathrm{RF}}^{\mathrm{H}} \mathbf{H}\mathbf{H}^{\mathrm{H}} \mathbf{W}_{\mathrm{RF}}\right), \tag{10}$$

where $\mathbf{R}_{\mathrm{n}_{\mathrm{RF}}} = \mathbf{W}_{\mathrm{RF}}^{\mathrm{H}} \mathbf{W}_{\mathrm{RF}}$ is the noise covariance matrix after analog processing.

From (10), it is apparent that different choices of $\mathbf{W}_{\mathrm{RF}}$ greatly affect the system performance. Note that the elements of $\mathbf{W}_{\mathrm{RF}}$ are related to the way how antennas are connected to RF chains by the phase shifter network. To find the optimal connection, we will focus on the analog processing matrix $\mathbf{W}_{\mathrm{RF}}$. For the sake of describing the case of connection between the antenna and the RF chains, inspired by Zhu et al. [35], the (n, m)-th element of $\mathbf{W}_{\mathrm{RF}}$ can be modeled as

$$\mathbf{W}_{\mathrm{RF}}(n, m) = \begin{cases} 1, & \text{the } n-\text{thantennaisconnected} \\ \text{withthe} & m-\text{thRFchain}, \\ 0, & \text{otherwise}, \end{cases} \tag{11}$$

where $n = 1, \cdots, N$ and $m = 1, \cdots, M$. It is worth mentioning that in general, the elements of $\mathbf{W}_{\mathrm{RF}}$ can be any complex value with unit norm (i.e., $\mathbf{W}_{\mathrm{RF}}(n, m) = \mathrm{e}^{\mathrm{j}\theta_{\mathrm{nm}}}$). To concentrate on the connection structure, they are assumed to be binary here. To describe the arbitrary connection between the antenna array and the RF connections, we use the connection model (11). For example, when the whole elements in $\mathbf{W}_{\mathrm{RF}}$ are

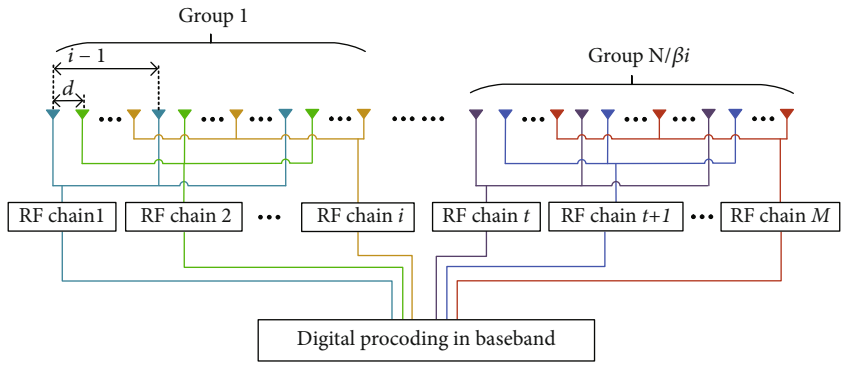

Figure 2: Interleaved structure.

equal to one, it is actually a fully connected structure. When $\mathbf{W}_{\mathrm{RF}}$ is a block diagonal matrix, it represents the localized structure [14–17]. In this work, we aim to optimize the interleaved structure which has gained great research interest and is shown to provide superior performance [20, 29, 31].

As shown in Figure 2, it is the interleaved structure. N antennas are uniformly parted into M antenna subarrays, so that $\beta = N/M$ antennas belong to one subarray and connect to the same RF chain. We denote i as the interleaved factor. Limited to the structure, i ought to be a divisor of K. There are $i-1$ antennas between two consecutive antennas of the same subarray. Therefore, the distance of them is $(i-1)d$. To elaborate on the interleaved structure from another perspective, i RF chains and the βi antennas connected to them form a group. Therefore, the antenna arrays are parted into $N/\beta i$ groups. In Figure 2, t is the index of the first RF chain of corresponding to the last group, and the value of t can be represented as $[N/\beta i - 1]i + 1$. From Figure 2, we know that each subarray's elements are dispersed through the antenna array group. When $i = 1$, it means that two consecutive antennas in the same subarray are separated by $i - 1 = 0$ antenna element, which is actually the localized structure [31].

Diverse interleaved structures could be described by the aforementioned model. Solving the following problem can yield the optimal structure, i.e., the optimal W_{RF}.

$$\begin{aligned}\mathbf{W}_{\mathrm{RF}}^{*} &= \arg \max_{\mathbf{W}_{\mathrm{RF}} \in \mathbb{B}^{N\times M}} I(s, y_{\mathrm{RF}}),\\ (\mathrm{a}) &\sum_{n=1}^{N} \mathbf{W}_{\mathrm{RF}}(n, m) = \beta,\\ (\mathrm{b}) &\mathbf{W}_{\mathrm{RF}}\left(n_{m,p}, m\right) = 1,\\ &n_{m,p+1} - n_{m,p} = i,\end{aligned} \tag{12}$$

where $\mathbb{B}\Delta = \{0, 1\}$, and (a) indicates that there are β elements equal to one in each column of W_{RF}. In (b), $n_{m,p}$ represents the index of the p-th 1-valued element in the m-th column, and $p \in \{1, 2, \cdots, \beta - 1\}$. Constraint b) means that two continuous 1-valued elements in a column are separated by $i - 1$ elements.

The optimization objective involves expectation, (12) is discrete, resulting in a nonconvex optimization problem, and thus the globally optimal solution of (12) is very difficult.

3. Suboptimal Design of the Interleaved Structure

In this section, we derive a closed form suboptimal solution to (12) by leveraging the properties of the mmWave channels.

According to (11), we have $\mathbf{R}_{\mathrm{n_{RF}}} = \beta \mathbf{I}_M$, and thus the mutual information can be written as

$$I(s, y_{\mathrm{RF}}) = \mathbb{E} \log_2 \det\left(\mathbf{I}_K + p\beta^{-1}\mathbf{W}_{\mathrm{RF}}^{\mathrm{H}}\mathbf{H}\mathbf{H}^{\mathrm{H}}\mathbf{W}_{\mathrm{RF}}\right). \tag{13}$$

Applying Jensen's inequality results in

$$I(s, y_{\mathrm{RF}}) \le \mathrm{F}\left(K, p, \beta, i, \frac{d}{\lambda}\right) \triangleq \log_2 \mathbb{E} \det\left(\mathbf{I}_K + p\beta^{-1}\mathbf{W}_{\mathrm{RF}}^{\mathrm{H}}\mathbf{H}\mathbf{H}^{\mathrm{H}}\mathbf{W}_{\mathrm{RF}}\right). \tag{14}$$

Problem (12) is changed to optimize the upper bound and we have.

$$\begin{aligned}\mathbf{W}_{\mathrm{RF}}^{*} = \arg &\max_{\mathbf{W}_{\mathrm{RF}} \in \mathbb{B}^{N\times M}} \mathrm{F}\left(K, p, \beta, i, \frac{d}{\lambda}\right)\\ &\mathrm{s.t.a), b) in (12)},\end{aligned} \tag{15}$$

by taking advantage of the characteristics of the mmWave channel, the $(\tilde{k}, k)$-th element of $\mathbf{W}_{\mathrm{RF}}^{\mathrm{H}}\mathbf{H}$ in (14) is given by

$$\mathbf{W}_{\mathrm{RF}}^{\mathrm{H}}\mathbf{H}\left(\tilde{k}, k\right) = \frac{1}{\sqrt{L}} \sum_{l=1}^{L} \alpha_{kl} \mathrm{e}^{-\mathrm{j}2\pi \mathrm{S}\left(\tilde{k}, i\right) d/\lambda \cos \phi_{kl}} \left(\sum_{m=0}^{\beta-1} \mathrm{e}^{-\mathrm{j}2\pi m i d/\lambda \cos \phi_{kl}}\right), \tag{16}$$

where $\tilde{k}$ and k can be any integer from 1 to K.Then, we write $\mathrm{S}(\tilde{k}, i)$ (16)

$$\mathrm{S}\left(\tilde{k}, i\right) = \mathrm{R}\left(\tilde{k}, i\right) + \mathrm{I}\left(\tilde{k}, i\right) i\beta, \tag{17}$$

where $\mathrm{I}(\tilde{k}, i) = \lfloor \tilde{k} - 1/i \rfloor$ denotes the largest integer not more than $\tilde{k} - 1/i$, and $\mathrm{R}(\tilde{k}, i) = \tilde{k} - 1 - \mathrm{I}(\tilde{k}, i)i$ denotes to the remainder of $(\tilde{k} - 1)/i$. Since (16) is very complicated and contains multiple propagation paths, it is not easy to solve (15) directly. Therefore, we first consider $L = 1$, which means that there is only one effective propagation path available for each user, and then the results are extended to cases with $L > 1$.

3.1. Solution for $L = 1$. Assuming $L = 1$ and from (16), we have

$$\mathbf{W}_{\mathrm{RF}}^{\mathrm{H}}\mathbf{H}\left(\tilde{k}, k\right) = \alpha_{k1}\mathrm{e}^{-\mathrm{j}2\pi\mathrm{S}\left(\tilde{k},i\right)d/\lambda\,\cos\,\phi_{k1}}\left(\sum_{m=0}^{\beta-1}\mathrm{e}^{-\mathrm{j}2\pi mid/\lambda\,\cos\,\phi_{k1}}\right). \tag{18}$$

By some mathematical manipulations, $\mathbf{W}_{\mathbf{RF}}^{\mathbf{H}}\mathbf{H}$ can be rewritten as

$$\mathbf{W}_{\mathbf{RF}}^{\mathbf{H}}\mathbf{H} = \tilde{H}V, \tag{19}$$

where $\tilde{\mathbf{H}} \in \mathbb{C}^{K\times K}$ and the $(\tilde{k}, k)$-th element is given by

$$\mathbf{H}\left(\tilde{k}, k\right) = \mathrm{e}^{-\mathrm{j}2\pi\mathrm{S}\left(\tilde{k},i\right)d/\lambda\,\cos\,\phi_{k1}}. \tag{20}$$

In (19), $\mathbf{V}$ is a diagonal matrix, and the k-th diagonal element is provided by

$$\mathbf{V}(k, k) = \alpha_{k1}\left(\sum_{m=0}^{\beta-1}\mathrm{e}^{-\mathrm{j}2\pi mid/\lambda\,\cos\,\phi_{k1}}\right). \tag{21}$$

Substituting (19) into (14) yields

$$\begin{aligned}\mathrm{F}_1(K, p, \beta, i, d/\lambda)\Delta &= \log_2\mathbb{E}\,\det\left(\mathbf{I}_K + p\beta^{-1}\tilde{\mathbf{H}}\mathbf{V}\mathbf{V}^{\mathrm{H}}\tilde{\mathbf{H}}^{\mathrm{H}}\right)\\ &\overset{(a)}{\approx} \log_2\mathbb{E}\,\det\left[\frac{1}{K}\tilde{\mathbf{H}}^{\mathrm{H}}\left(I_K + p\beta^{-1}\tilde{\mathbf{H}}\mathbf{V}\mathbf{V}^{\mathrm{H}}\tilde{\mathbf{H}}^{\mathrm{H}}\right)\tilde{\mathbf{H}}\right]\\ &\overset{(b)}{\approx} \log_2\mathbb{E}\,\det\left(\mathbf{I}_K + Kp\beta^{-1}\mathbf{V}\mathbf{V}^{\mathrm{H}}\right),\end{aligned} \tag{22}$$

where (a) and (b) follow $\tilde{\mathbf{H}}^{\mathrm{H}}\tilde{\mathbf{H}} \approx K\mathbf{I}_K$. Note that $\tilde{\mathbf{H}}^{\mathrm{H}}\tilde{\mathbf{H}} \neq K\mathbf{I}_K$ generally. However, a characteristic of large random matrices states that the columns of $\mathbf{H}$ become asymptotically orthogonal when K is large, which results in $\tilde{\mathbf{H}}^{\mathrm{H}}\tilde{\mathbf{H}} \approx K\mathbf{I}_K$. The average correlation coefficient of two different columns of $\tilde{\mathbf{H}}$ decreases as the amount of K increases, as in Figure 3. Hence, F_1 can be further simplified with (19) as

$$\begin{aligned}\mathrm{F}_1\left(K, p, \beta, i, \frac{d}{\lambda}\right) &\approx \log_2\mathbb{E}\,\det\left(\mathbf{I}_K + Kp\beta^{-1}\mathbf{V}\mathbf{V}^{\mathrm{H}}\right)\\ &= \log_2\prod_{k=1}^{K}\left[1 + Kp\beta^{-1}\mathbb{E}|\alpha_{k1}|^2\mathrm{L}_1\left(\beta, i, \frac{d}{\lambda}\right)\right],\end{aligned} \tag{23}$$

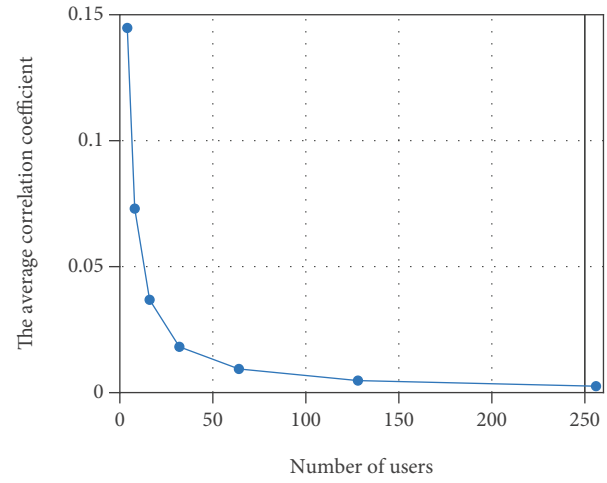

Figure 3: The average correlation coefficient of two different columns of $\tilde{\mathbf{H}}$.

where $\mathbb{E}|\alpha_{k1}|^2 = 1$, and $\mathrm{L}_1(\beta, i, (d/\lambda))$ is given by

$$\begin{aligned}\mathrm{L}_1\left(\beta, i, \frac{d}{\lambda}\right) &= \mathbb{E}\left[\left(\sum_{m=0}^{\beta-1}\mathrm{e}^{-\mathrm{j}2\pi mid/\lambda\,\cos\,\phi_{k1}}\right)\left(\sum_{m=0}^{\beta-1}\mathrm{e}^{\mathrm{j}2\pi mid/\lambda\,\cos\,\phi_{k1}}\right)\right]\\ &= \beta + \sum_{m=1}^{\beta-1}2(\beta - m)\mathbb{E}\cos\left(2\pi mid/\lambda\,\cos\,\phi_{k1}\right)\\ &\overset{(a)}{=} \beta + \sum_{m=1}^{\beta-1}(\beta - m)\frac{1}{\pi}\int_{-\pi}^{\pi}\cos\left(2\pi mid/\lambda\,\cos\,\phi_{k1}\right)\mathrm{d}\phi_{k1}\\ &\overset{(b)}{=} \beta + \sum_{m=1}^{\beta-1}2(\beta - m)\mathrm{J}_0\left(2\pi mi\frac{d}{\lambda}\right),\end{aligned} \tag{24}$$

where (a) follows

$$\mathbb{E}\cos\left(2\pi mi\frac{d}{\lambda}\cos\,\phi_{k1}\right) = \frac{1}{2\pi}\int_{-\pi}^{\pi}\cos\left(2\pi mi\frac{d}{\lambda}\cos\,\phi_{k1}\right)\mathrm{d}\phi_{k1}, \tag{25}$$

and (b) is obtained by using

$$\int_0^1\frac{\cos\,(ax)}{\sqrt{1 - x^2}}dx = \frac{\pi}{2}\mathrm{J}_0(a). \tag{26}$$

Substituting (24) into (23), F_1 is given by

$$\mathrm{F}_1\left(K, p, \beta, i, \frac{d}{\lambda}\right) = K\log_2\left[1 + Kp\beta^{-1}\mathrm{L}_1\left(\beta, i, \frac{d}{\lambda}\right)\right], \tag{27}$$

in which F_1 is simplified to be a function of K, p, β, i and d/λ. For given K, p, β and d/λ, (15) can be simplified into the following problem:

$$i^* = \arg\ \max\ \mathrm{F}_1(i)\ \text{s.t.}\ i\ \text{is adivisor of}\ K. \tag{28}$$

Then, (28) is equivalent to

$$\max_{i^*} \mathrm{L}_1(i) \Leftrightarrow \max_{i^*} \beta + \sum_{m=1}^{\beta-1} 2(\beta - m)\mathrm{J}_0\left(2\pi m i \frac{d}{\lambda}\right) \text{ s.t.} i \text{ is adivisor of } K. \tag{29}$$

Since $\mathrm{L}_1(i)$ contains a summation of weighted Bessel functions, the recursive formula of zero-order Bessel function is used to find the optimal value of i. The derivative of $L_1(i)$ is obtained as

$$\mathrm{L}_1'(i) = -\left[\sum_{m=1}^{\beta-1} 4\pi m \frac{d}{\lambda}(\beta - m)\mathrm{J}_1\left(2\pi m i \frac{d}{\lambda}\right)\right]. \tag{30}$$

Denote i^* as the solution to $\mathrm{L}_1'(i) = 0$, and we obtain the following theorem.

Theorem 1. *When the system has a large number of users and each user has only one valid propagation path $(L = 1)$, the optimal interleaved structure is satisfied $L_1'(i^*) = 0$.*

Theorem 1 provides a sufficient condition for the optimal interleaved structure. However, the solution of $\mathrm{L}_1'(i^*) = 0$ is not easy to obtain in general. Therefore, to gain more insights, we analyze some special cases in the following corollaries.

Corollary 2. *In a particular case, when each subarray contains only two antenna elements, i.e., $\beta = 2$, supposing that $d/\lambda = 1/2$, the interleaved structure that maximizes the spectral efficiency requires $i^* = 2$.*

Substituting $\beta = 2$ into (30) and setting it to zero, we have

$$-4\pi \frac{d}{\lambda}\mathrm{J}_1\left(2\pi i \frac{d}{\lambda}\right) = 0. \tag{31}$$

Based on the asymptotic expansion of the first order Bessel function $J_1(X)$, the zero point is $X^* \approx (q + 1/4)\pi$, where $q = 1, 2, 3, \cdots$ Since $d/\lambda = 1/2$, the solution to (31) is approximated by

$$i^* \approx q + \frac{1}{4}. \tag{32}$$

When q is even, i^* is the locally maximum point of the function $L_1(i)$. Because the first-order Bessel function varies and disappears, $L_1(i)$ achieves the maximum when $q = 2$, i.e., $i^* \approx 2.25$. However, considering the actual situation, i is the divisor of user number, the interleaved structure of $i^* = 2$ can be realized, and the value of $L_1(i)$ is the largest at this time.

Corollary 3. *In more general cases, for that β is an integer greater than 1, when $d/\lambda = 1/2$, the interleaved structures that maximizes the spectral efficiency should satisfy $i^* = 2$.*

Although the first-order Bessel function $J_1(X)$ is not periodic, the zero points of the first-order Bessel function $J_1(X)$ tend to be periodic, i.e.,

$$\lim_{v \longrightarrow \infty} \mu_{v+1} - \mu_v = \pi, \tag{33}$$

where μ_v is the nonnegative zero point of $J_1(X)$, $v = 1, 2, \cdots$ When X is small, the distance between two adjacent zero points is close to π. Therefore, its period is infinitely close to 2π. Assuming $d/\lambda = 1/2$, the period of $J_1(2\pi m i(d/\lambda))$ is approximately equal to $2/m$. Note that $\mathrm{L}_1'(i)$ is a summation of multiple weighted first-order Bessel functions. According to the addition principle of the periodic function, the period of the sum is equal to the least common multiple of the period of each term in the summation. Therefore, the approximate period of $L_1'(i)$ is 2. Besides, according to the expansion of the Bessel function, $i^* \approx 2$ could make each term, i.e., $\mathrm{J}_1(2\pi m i(d/\lambda))$ in $L_1'(i)$ equals zero. In other words, $i^* \approx 2$ is the solution of $L_1'(i) = 0$. The locally maximum point of $L_1(i)$ is obtained. Limited to the interleaved structure, i^* ought to be 2.

For the case of multiple effective propagation paths, more results are provided in the following subsection.

3.2. Solution for $L > 1$. Consider that each user's channel contains multiple valid propagation paths, i.e., $L > 1$. According to (16), $W_{\mathrm{RF}}^{\mathrm{H}} H$ can be expressed as

$$W_{\mathrm{RF}}^{\mathrm{H}} H = \sum_{l=1}^{L} \left(W_{\mathrm{RF}}^{\mathrm{H}} H\right)_l, \tag{34}$$

where $\left(W_{\mathrm{RF}}^{\mathrm{H}} H\right)_l$ represents the component corresponding to the l-th path in $W_{\mathrm{RF}}^{\mathrm{H}} H$. Similar to the case when $L = 1$, $\left(W_{\mathrm{RF}}^{\mathrm{H}} H\right)_l$ is decomposed into

$$\left(W_{\mathrm{RF}}^{\mathrm{H}} H\right)_l = \tilde{H}_l V_l, \tag{35}$$

where $\tilde{H}_l \in \mathbb{C}^{K \times K}$ and the $(\tilde{k}, k)$-th element is defined as

$$\tilde{H}_l\left(\tilde{k}, k\right) = \frac{1}{\sqrt{L}} \mathrm{e}^{-\mathrm{j}2\pi \mathrm{S}\left(\tilde{k}, i\right) d/\lambda \cos \phi_{kl}}. \tag{36}$$

Moreover, $\mathbf{V}_l \in \mathbb{C}^{K \times K}$ is a diagonal matrix, and the (k, k)-th element of $\mathbf{V}_l$ is

$$\mathbf{V}_l(k, k) = \alpha_{kl}\left(\sum_{m=0}^{\beta-1} \mathrm{e}^{-\mathrm{j}2\pi m i d/\lambda \cos \phi_{kl}}\right). \tag{37}$$

To simplify the derivation, F_2 in (14) can be further deduced to

$$F_2\left(K, p, \beta, i, \frac{d}{\lambda}\right), \quad \log_2 \mathbb{E} \det\left(I_K + p\beta^{-1} H^{\mathrm{H}} W_{\mathrm{RF}} W_{\mathrm{RF}}^{\mathrm{H}} H\right). \tag{38}$$

Input: N, K, p, and d/λ;
1: Calculate the number of antennas in one Subarray $\beta \longleftarrow N/K$;
2:Calculate the divisors of K and denote as a set. $\mathcal{D} = \{d_1, d_2, \cdots, d_Z\}$, where Z is the number of the divisors of K;
3: For $i \in \mathcal{D}$ do:
4: Calculate $r(i) \longleftarrow K \log_2[1 + LKp\beta^{-1}\mathrm{L}_2(i)]$;
5: $r_z \longleftarrow r(i), z = 1, 2, \cdots, Z$;
6: End;
7:Find $r_{\max} \longleftarrow \max\ \{r_1, r_2, \cdots, r_Z\}$;
8: $z^* \longleftarrow$ the index of $r_{\max}$;
9: The optimal interleaved structure parameter is $i^* \longleftarrow d_{z^*}$
Output: i^*.

Algorithm 1: The proposed ODS algorithm.

According to (34) and (35), F_2 can be rewritten as

$$\log_2 \mathbb{E} \det \left[\mathbf{I}_K + p\beta^{-1} \left(\sum_{l=1}^{L} \tilde{\mathbf{H}}_l V_l \right)^{\mathrm{H}} \left(\sum_{l=1}^{L} \tilde{\mathbf{H}}_l \mathbf{V}_l \right) \right], \tag{39}$$

where

$$\left(\sum_{l=1}^{L} \tilde{H}_l V_l \right)^{\mathrm{H}} \left(\sum_{l=1}^{L} \tilde{H}_l V_l \right) = \underbrace{\left\{ \sum_{l=1}^{L} \left(\tilde{H}_l V_l \right)^{\mathrm{H}} \left(\tilde{H}_l V_l \right) \right\}}_{\text{same path}} + \underbrace{\left\{ \sum_{i,j=1\ i \neq j}^{L} \left(\tilde{H}_i V_i \right)^{\mathrm{H}} \left(\tilde{H}_j V_j \right) \right\}}_{\text{different path}}, \tag{40}$$

where the first part is the component of the same path in the equivalent channel $W_{\mathrm{RF}}^{\mathrm{H}} H$, and the second part is the mutual interference between different paths. Since different paths are independent of each other, when the number of antennas is large, the mutual interference between different paths is approximately to be zero. Then, F_2 is approximated by

$$\mathrm{F}_2(K, p, \beta, i, d/\lambda) \approx \log_2 \mathbb{E} \det \left\{ I_K + p\beta^{-1} \left[\sum_{l=1}^{L} \left(\tilde{H}_l V_l \right)^{\mathrm{H}} \left(\tilde{H}_l V_l \right) \right] \right\}. \tag{41}$$

Since $\tilde{\mathbf{H}}_l^{\mathrm{H}} \tilde{\mathbf{H}}_l \approx K I_K$, it yields

$$\mathrm{F}_2(K, p, \beta, i, d/\lambda) \approx \log_2 \mathbb{E} \det \left[I_K + p\beta^{-1} K \left(\sum_{l=1}^{L} \mathbf{V}_l \mathbf{V}_l^{\mathrm{H}} \right) \right]. \tag{42}$$

It is worth pointing out that the approximation from (41) to (42) is valid when N, K goes to infinity, and it becomes less accurate for the limited value of N and K. However, this approximation simplifies the analysis, and the obtained optimal interleaved structure works well under moderate values of N and K. According to (37) and (42), for given $K, p, \beta, d/\lambda$, F_2 is rewritten as

$$\mathrm{F}_2(i) \approx \log_2 \prod_{k=1}^{K} \left\{ 1 + Kp\beta^{-1} \sum_{l=1}^{L} \left[\mathbb{E}|\alpha_{kl}|^2 \mathrm{L}_2(i) \right] \right\}, \tag{43}$$

where $\mathbb{E}|\alpha_{kl}|^2 = 1$, and $\mathrm{L}_2(i)$ is defined as

$$\begin{aligned} \mathrm{L}_2(i) &= \mathbb{E} \left[\left(\sum_{m=0}^{\beta-1} \mathrm{e}^{-\mathrm{j}2\pi \mathrm{mid}/\lambda \cos \phi_{kl}} \right) \left(\sum_{m=0}^{\beta-1} \mathrm{e}^{\mathrm{j}2\pi \mathrm{mid}/\lambda \cos \phi_{kl}} \right) \right] \\ &= \beta + \sum_{m=1}^{\beta-1} 2(\beta - m) \mathbb{E} \cos \left(2\pi \mathrm{mi} \frac{\mathrm{d}}{\lambda} \cos \phi_{kl} \right), \end{aligned} \tag{44}$$

in which $\mathbb{E} \cos (2\pi \mathrm{mi}(d/\lambda) \cos \phi_{kl})$ is given by

$$\mathbb{E} \cos \left(2\pi \mathrm{mi} \frac{d}{\lambda} \cos \phi_{kl} \right) = \mathrm{J}_0 \left(2\pi \mathrm{mi} \frac{d}{\lambda} \right). \tag{45}$$

It can be seen that $L_2(i)$ is independent of ϕ_{kl}, while it is related to i. (44) is rewritten as

$$\mathrm{L}_2(i) = \beta + \sum_{m=1}^{\beta-1} 2(\beta - m) \mathrm{J}_0 \left(2\pi mi \frac{d}{\lambda} \right), \tag{46}$$

Note that L_2 in (46) is equal to L_1 in (24). With (43) and (46), the objective function F_2 is eventually simplified to

$$\mathrm{F}_2(i) = K \log_2 \left[1 + LKp\beta^{-1} \mathrm{L}_2(i) \right]. \tag{47}$$

It is observed that F_2 is related to i, and then the optimization problem (15) is simplified as

$$i^* = \arg \max F_2(i) \text{ s.t.} i \text{ is the divisor of } K. \tag{48}$$

Because the optimization objective is a nonconvex function of i, the optimization problem is complicated to solve. In this work, we propose to solve (48) by Algorithm 1. It

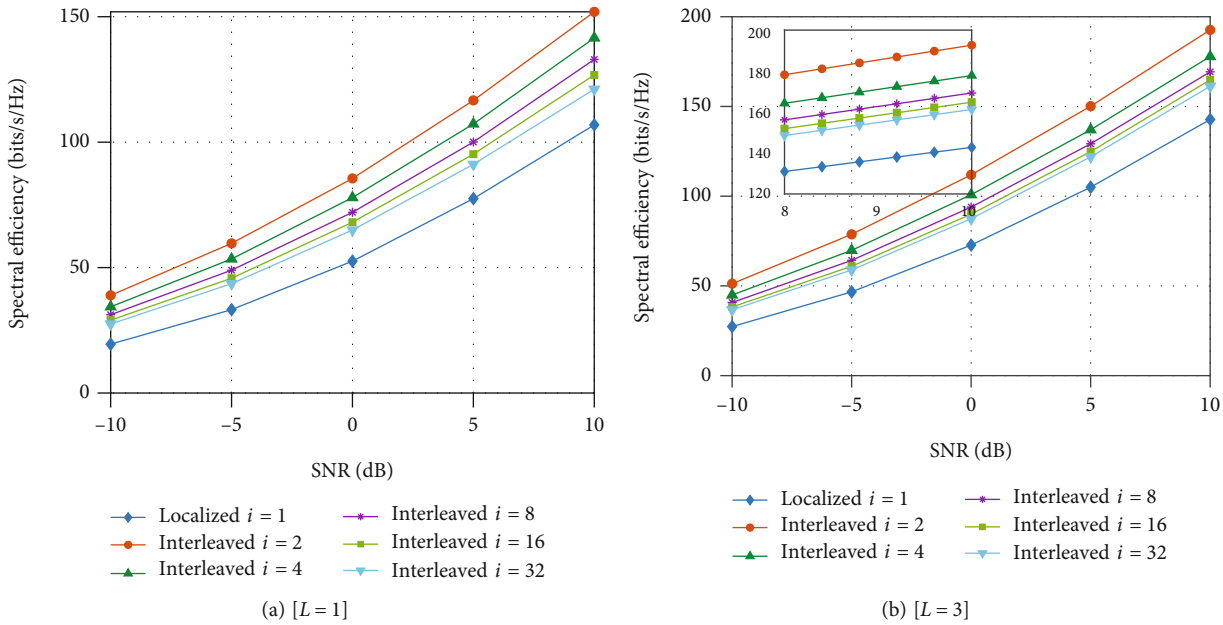

FIGURE 4: Spectral efficiency achieved by various interleaved structures when the number of RF chains is 32.

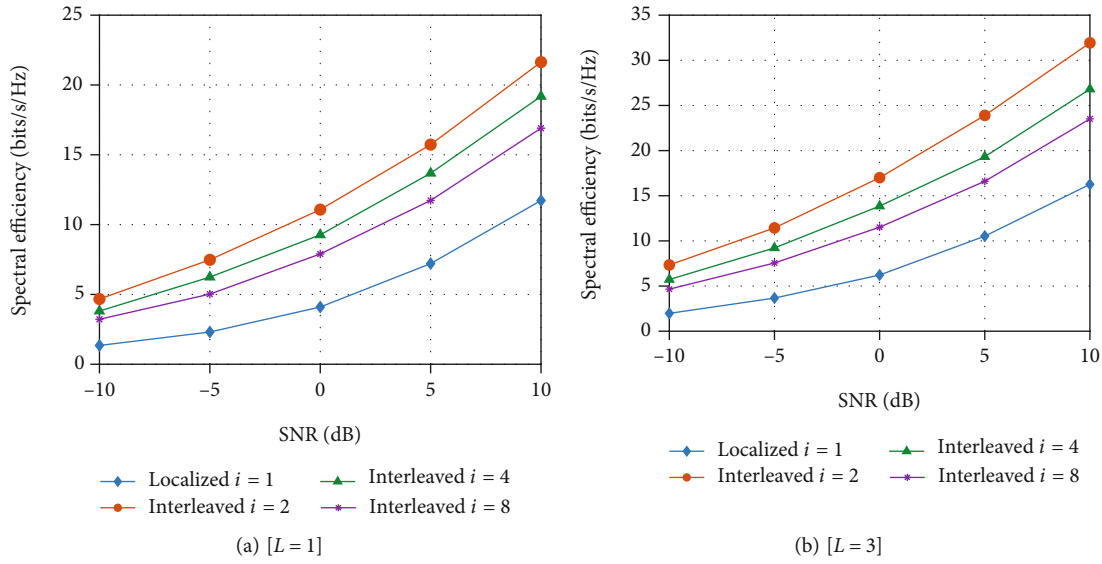

FIGURE 5: Spectral efficiency achieved by various interleaved structures when the number of RF chains is 8.

calculates and compares the values of F_2 to obtain the optimal parameter that maximizes F_2.

4. Numerical Results

In this section, the numerical results are presented to demonstrate the performance of various subconnected structures in terms of the spectral efficiency. In simulations, the number of BS antennas is 256, and the number of RF chains is 8 or 32. Two cases of $L = 1$ and $L = 3$ are considered, respectively. The AoAs are assumed to be uniformly distributed in $(0, 2\pi]$. p is referred to as signal-to-noise ratio (SNR).

Under the condition that $d = \lambda/2$, when the RF chains is 32, the achievable spectral efficiency performance of diverse interleaved structures with variational SNR for $L = 1$ and $L = 3$ is illustrated in Figure 4(a) and 4(b), respectively. As shown in Figure 4(a), the interleaved structure obtains the maximum spectral efficiency when $i = 2$, which is followed by $i = 4, 8, 16, 32, 1$ in descending order of spectral efficiency. This verified the analysis in Section 3.1. The interleaved structure with $i = 1$ is actually the localized structure, which performs the worst. The same results can be found in Figure 5 where the number of RF chain in 8. Besides, the gap between interleaved and localized structures becomes larger as the SNR increases. In Figure 4(b), the spectral efficiency of various interleaved structures also increases as the SNR increases, and compared with Figure 4(a), the spectral efficiency is higher when $L = 3$ due to the increased order

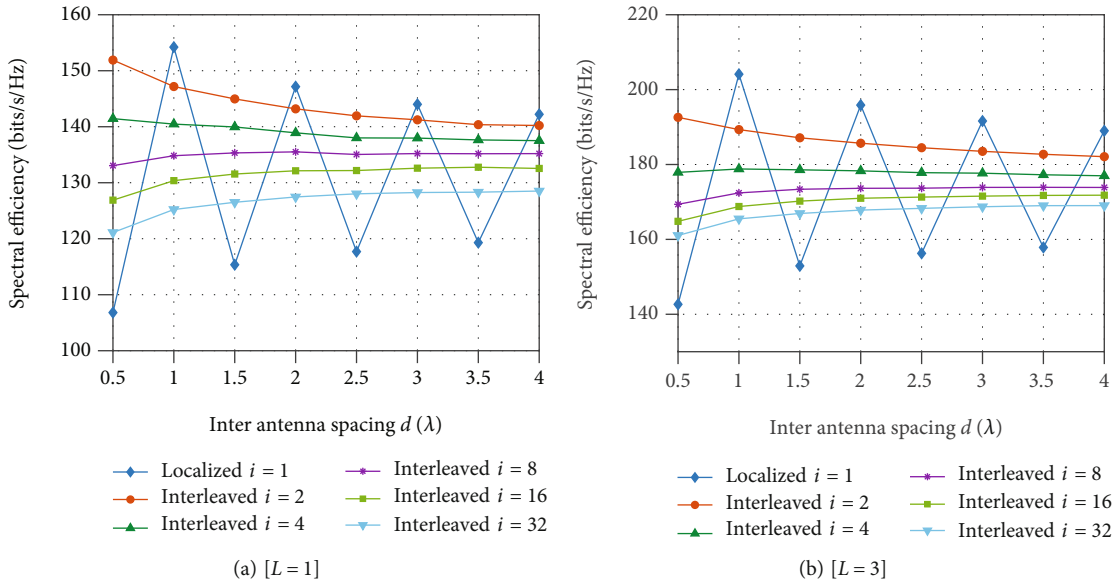

FIGURE 6: Spectral efficiency vs. d in a serious of interleaved structure where SNR = 10 dB when the number of RF chains is 32.

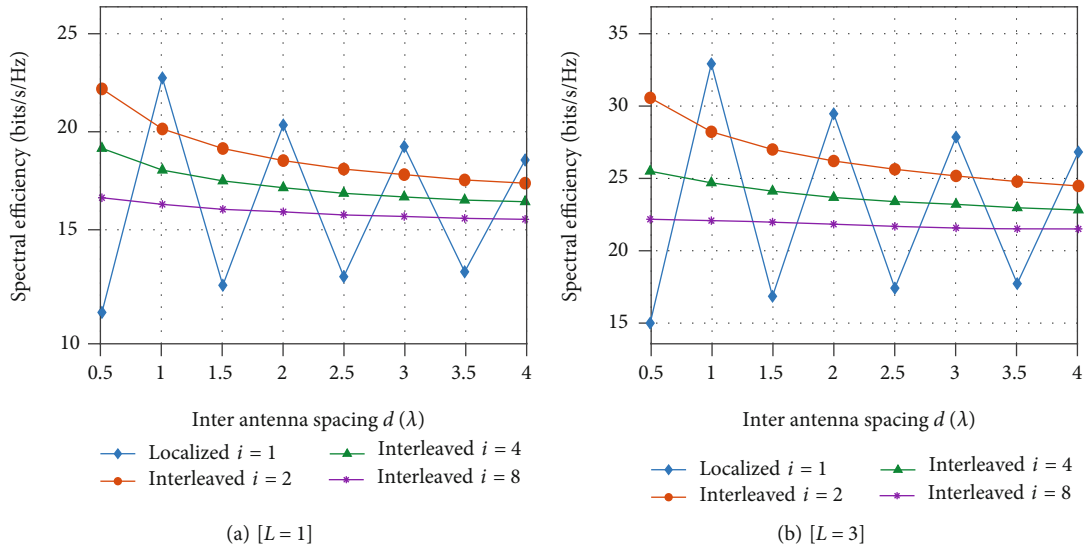

FIGURE 7: Spectral efficiency vs. d in a serious of interleaved structure where SNR = 10 dB when the number of RF chains is 8.

of freedom. When the SNR is fixed, various interleaved structures are ranked as $i = 2, 4, 8, 16, 32, 1$ in descending order of spectral efficiency. The interleaved structure achieves the maximum spectral efficiency when $i = 2$, which is in accordance with the output of Algorithm 1 with a linear complexity of $\mathcal{O}(Z)$. Similarly as $L = 1$, the spectral efficiency is the smallest when $i = 1$, i.e., the localized structure. The same results can be found in Figure 5 where the number of RF chain in 8.

Figure 6 shows a comparison of the spectral efficiency for different subconnected structures in regard to the interantenna spacing d in the case of $L = 1$ and $L = 3$, respectively. It is shown that the spectral efficiency of the interleaved structure with $i = 1$ fluctuates and attenuates as d increases, and the performance of $i = 2, 4, 8, 16, 32$ is in descending order. When d is an odd multiple of the half wavelength, i.e., $d = (2u + 1)\lambda/2$, $u = 0, 1, 2, \cdots$, the maximum spectral efficiency of the interleaved structure is obtained when $i = 2$, and the minimum is got when $i = 1$. However, when the interantenna distance d is an even multiple of the half wavelength, i.e., $d = (2u)\lambda/2$, we have $i = 1, 2, 4, 8, 16, 32$ in descending order of spectral efficiency. The same results as show in Figure 7 where the number of RF chain is 8. Figures 6(a) and 6(b) illustrate the connection between spectral efficiency and antenna array configuration, which provide help for the disposition of the mmWave massive MIMO antenna arrays.

Figure 8 shows the impact of the parameter of interleaved structure i on the spectral efficiency for $L = 1$ and $L = 3$, respectively. The interantenna spacing d is $\lambda/2$. According to the above theoretical analysis, the optimal interleaved structure is related to the number of users. The parameter i

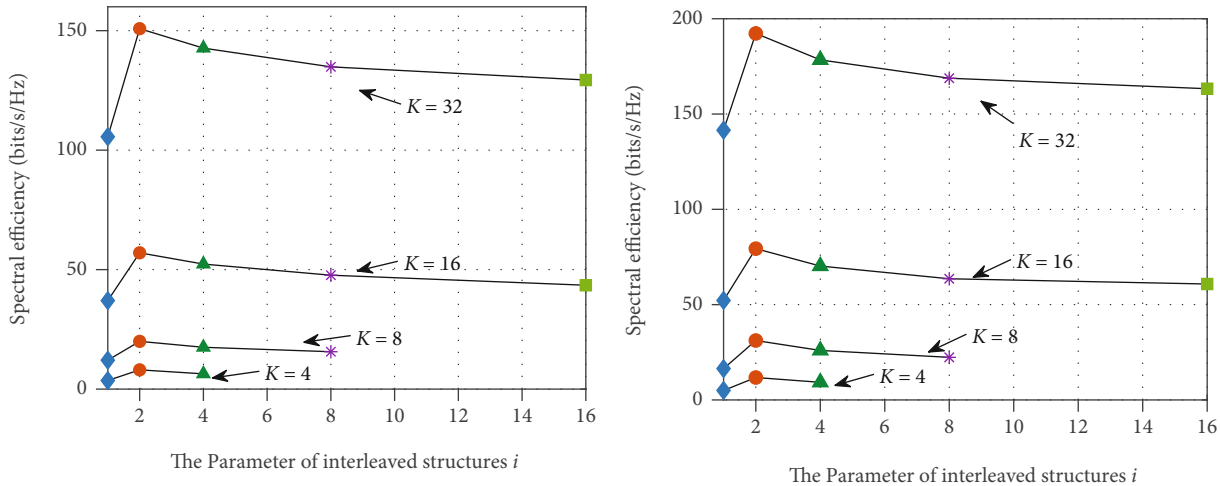

FIGURE 8: Spectral efficiency vs. the parameter of interleaved structures i for different number of users.

of the interleaved structure is a divisor of the number of users. For example, when the number of users is 32, there are five available interleaved structures, $i = 1, 2, 4, 8, 16, 32$. It can be drawn from the figure that the structure with the largest spectral efficiency requires $i = 2$. Algorithm 1 gives the same results.

5. Conclusion

This paper has studied the connection between the antennas and the RF chains for the hybrid structure in mmWave massive MIMO systems. We investigated the best design of an interleaved subconnected hybrid structure in two situations using the features of the mmWave channel. One is the case with only one propagation path from each user to the BS, and the other is with multiple propagation paths. With the goal of maximizing the spectrum efficiency, the suboptimal interleaved structure has been derived, and numerical results were verified during the analysis. When the interantenna spacing equals even multiples of half wavelength, the best spectral efficiency is obtained by the localized structure. When the interantenna spacing equals an odd multiple of half wavelength, the interleaved structure with $i = 2$ achieves the best performance.

Data Availability

The data used to support the funding of this study are included within the article.

Conflicts of Interest

The authors declare that they have no conflicts of interest.

Acknowledgments

This work was supported in part by the National Nature Science Foundation of China (Nos. 61701198 and 62171204), Nature Science Foundation of Jiangsu Province (No. BK20170557), and the Key Research & Development Plan of Jiangsu Province (No. BE2018108).

References

[1] X. Gu, W. Zhang, and X. Bao, "Optimal design of subconnected hybrid structure for mmwave massive mimo systems," in *in 2019 IEEE 19th International Conference on Communication Technology (ICCT)*, pp. 685–689, 2019.

[2] J. G. Andrews, S. Buzzi, C. Wan et al., "What will 5g be?," *IEEE Journal on Selected Areas in Communications*, vol. 32, no. 6, pp. 1065–1082, 2014.

[3] T. Bai, A. Alkhateeb, and R. W. Heath, "Coverage and capacity of millimeter-wave cellular networks," *IEEE Communications Magazine*, vol. 52, no. 9, pp. 70–77, 2014.

[4] W. Zhang, H. Ren, C. Pan et al., "Large-scale antenna systems with ul/dl hardware mismatch: achievable rates analysis and calibration," *IEEE Transactions on Communications*, vol. 63, no. 4, pp. 1216–1229, 2015.

[5] W. Zhang, R. C. de Lamare, C. Pan et al., "Widely linear precoding for large-scale mimo with iqi: algorithms and performance analysis," *IEEE Transactions on Wireless Communications*, vol. 16, no. 5, pp. 3298–3312, 2017.

[6] Z. Pi and F. Khan, "An introduction to millimeter-wave mobile broadband systems," *IEEE Communications Magazine*, vol. 49, no. 6, pp. 101–107, 2011.

[7] T. S. Rappaport, S. Shu, R. Mayzus et al., "Millimeter wave mobile communications for 5g cellular: it will work!," *IEEE Access*, vol. 1, no. 1, pp. 335–349, 2013.

[8] A. Rozé, M. Crussière, M. Hélard, and C. Langlais, "Comparison between a hybrid digital and analog beamforming system and a fully digital massive mimo system with adaptive beamsteering receivers in millimeter-wave transmissions," in *in 2016 International Symposium on Wireless Communication Systems (ISWCS)*, pp. 86–91, 2016.

[9] W. Zhang, X. Xia, Y. Fu, and X. Bao, "Hybrid and full-digital beamforming in mmwave massive mimo systems: a comparison considering low-resolution adcs," *China Communications*, vol. 16, no. 6, pp. 91–102, 2019.

[10] R. W. H. Jr, N. Gonzalezprelcic, S. Rangan, W. Roh, and A. Sayeed, "An overview of signal processing techniques for millimeter wave mimo systems," *IEEE Journal of Selected Topics in Signal Processing*, vol. 10, no. 3, pp. 436–453, 2016.

[11] O. E. Ayach, S. Rajagopal, S. Abu-Surra, Z. Pi, and R. W. Heath, "Spatially sparse precoding in millimeter wave mimo systems," *IEEE Transactions on Wireless Communications*, vol. 13, no. 3, pp. 1499–1513, 2014.

[12] R. Magueta, D. Castanheira, P. Pedrosa, A. Silva, R. Dinis, and A. Gameiro, "Iterative analog–digital multi-user equalizer for wideband millimeter wave massive mimo systems," *Sensors*, vol. 20, no. 2, p. 575, 2020.

[13] J. Kassam, M. Miri, R. Magueta et al., "Two-step multiuser equalization for hybrid mmwave massive mimo gfdm systems," *Electronics*, vol. 9, no. 8, p. 1220, 2020.

[14] X. Gao, L. Dai, S. Han, I. Chihlin, and R. W. H. Jr, "Energy-efficient hybrid analog and digital precoding for mmwave mimo systems with large antenna arrays," *IEEE Journal on Selected Areas in Communications*, vol. 34, no. 4, pp. 998–1009, 2016.

[15] N. Li, Z. Wei, H. Yang, X. Zhang, and D. Yang, "Hybrid precoding for mmwave massive mimo systems with partially connected structure," *IEEE Access*, vol. 5, pp. 15142–15151, 2017.

[16] Z. Zhang, X. Wu, and D. Liu, "Joint precoding and combining design for hybrid beamforming systems with subconnected structure," *IEEE Systems Journal*, vol. 14, no. 1, pp. 184–195, 2020.

[17] X. Liu, X. Li, S. Cao et al., "Hybrid precoding for massive mmwave mimo systems," *IEEE Access*, vol. 7, pp. 33577–33586, 2019.

[18] Z. Li, A. Honda, T. Shimura et al., "Multi-user mmwave communication by interleaved beamforming with inter-subarray coding," in *in 2017 IEEE 28th Annual International Symposium on Personal, Indoor, and Mobile Radio Communications (PIMRC)*, pp. 1–6, 2017.

[19] J. Zhang, W. Liu, C. Gu, S. S. Gao, and Q. Luo, "Two-beam multiplexing with inter-subarray coding for arbitrary directions based on interleaved subarray architectures," in *in 2019 IEEE 30th Annual International Symposium on Personal, Indoor and Mobile Radio Communications (PIMRC)*, pp. 1–5, 2019.

[20] S. Fujio and M. Shimizu, "Low-complexity scheduling method for interleaved hybrid beamforming in mmwave communications," in *in 2018 IEEE 29th Annual International Symposium on Personal, Indoor and Mobile Radio Communications (PIMRC)*, pp. 1–5, 2018.

[21] M. Wang, J. Cai, F. Tseng, and C. Hsu, "A low-complexity 2-d angle of arrival estimation in massive mimo systems," in *in 2016 International Computer Symposium (ICS)*, pp. 710–713, 2016.

[22] H. Li, T. Q. Wang, and X. Huang, "Joint adaptive aoa and polarization estimation using hybrid dual-polarized antenna arrays," *IEEE Access*, vol. 7, pp. 76353–76366, 2019.

[23] H. Li, T. Q. Wang, X. Huang, J. A. Zhang, and Y. J. Guo, "Low-complexity multiuser receiver for massive hybrid array mmwave communications," *IEEE Transactions on Communications*, vol. 67, no. 5, pp. 3512–3524, 2019.

[24] M. Shimizu, A. Honda, S. Ishikawa et al., "Millimeter-wave beam multiplexing method using hybrid beamforming," in *in 2016 IEEE 27th Annual International Symposium on Personal, Indoor, and Mobile Radio Communications (PIMRC)*, pp. 1–6, 2016.

[25] T. Shimura, T. Ohshima, H. Ashida et al., "Millimeter-wave tx phased array with phase adjusting function between transmitters for hybrid beamforming with interleaved subarrays," in *in 2016 46th European Microwave Conference (EuMC)*, pp. 1572–1575, 2016.

[26] S. Fujio, C. Kojima, T. Shimura et al., "Robust beamforming method for sdma with interleaved subarray hybrid beamforming," in *in 2016 IEEE 27th Annual International Symposium on Personal, Indoor, and Mobile Radio Communications (PIMRC)*, pp. 1–5, 2016.

[27] C. C. Hu and J. H. Zhang, "Hybrid precoding design for adaptive subconnected structures in millimeter-wave mimo systems," *IEEE Systems Journal*, vol. 13, no. 1, pp. 137–146, 2019.

[28] Z. Wang, J. Zhu, J. Wang, and G. Yue, "An overlapped subarray structure in hybrid millimeter-wave multi-user mimo system," in *in 2018 IEEE Global Communications Conference (GLOBECOM)*, pp. 1–6, 2018.

[29] X. Huang, Y. J. Guo, and J. D. Bunton, "A hybrid adaptive antenna array," *IEEE Transactions on Wireless Communications*, vol. 9, no. 5, pp. 1770–1779, 2010.

[30] X. Huang and Y. J. Guo, "Frequency-domain aoa estimation and beamforming with wideband hybrid arrays," *IEEE Transactions on Wireless Communications*, vol. 10, no. 8, pp. 2543–2553, 2011.

[31] J. A. Zhang, X. Huang, V. Dyadyuk, and Y. J. Guo, "Massive hybrid antenna array for millimeter-wave cellular communications," *IEEE Wireless Communications*, vol. 22, no. 1, pp. 79–87, 2015.

[32] S. A. Busari, K. M. S. Huq, S. Mumtaz, L. Dai, and J. Rodriguez, "Millimeter-Wave massive mimo communication for future wireless systems: a survey," *IEEE Communications Surveys Tutorials*, vol. 20, no. 2, pp. 836–869, 2018.

[33] S. Park, A. Alkhateeb, and R. W. Heath, "Dynamic subarrays for hybrid precoding in wideband mmwave mimo systems," *IEEE Transactions on Wireless Communications*, vol. 16, no. 5, pp. 2907–2920, 2017.

[34] M. A. Teeti, R. Wang, and R. Abdolee, "On the uplink achievable rate for massive mimo with 1-bit adc and superimposed pilots," *IEEE Access*, vol. 6, pp. 37627–37643, 2018.

[35] H. Zhu, F. Yang, Z. Zhu, and X. Luo, "Optimal interconnection for massive mimo self-calibration," in *in 2018 IEEE International Conference on Communications (ICC)*, pp. 1–6, 2018.